Experimental investigation of spin-orbit coupling in *n*-type PbTe quantum wells

M. L. Peres,[1] H. S. Monteiro,[1] V. A. Chitta,[2] S. de Castro,[1] U. A. Mengui,[3] P. H. O. Rappl,[3] N. F. Oliveira, Jr.,[2] E. Abramof,[3] and D. K. Maude[4]

[1]*Institute of Physics and Chemistry, Federal University of Itajubá, PB 50, 37500-903 Itajubá, MG, Brazil*
[2]*Institute of Physics, University of São Paulo, PB 66318, 05315-970 São Paulo, SP, Brazil*
[3]*Laboratório Associado de Sensores e Materiais, Instituto Nacional de Pesquisas Espaciais, PB 515, 12201-970 São José dos Campos, SP, Brazil*
[4]*Grenoble High Magnetic Field Laboratory, CNRS, BP 166, 38042 Grenoble Cedex 9, France*

The spin-orbit coupling is studied experimentally in two PbTe quantum wells by means of weak antilocalization effect. Using the Hikami-Larkin-Nagaoka model through a computational global optimization procedure, we extracted the spin-orbit and inelastic scattering times and estimated the strength of the zero field spin-splitting energy Δ_{so}. The values of Δ_{so} are linearly dependent on the Fermi wave vector (k_F) confirming theoretical predictions of the existence of large spin-orbit coupling in IV-VI quantum wells originated from pure Rashba effect. © *2014 AIP Publishing LLC.* [http://dx.doi.org/10.1063/1.4867627]

I. INTRODUCTION

The spin–orbit (SO) coupling for electrons in semiconductors nanostructures has been considered as one of the basis for new spintronic devices and has attracted much attention in the last two decades.[1–6] In particular, some effort has been dedicated to the development of a spin-based field effect transistor[6] leading to the investigation of the main issues concerning the determination of SO coupling in different systems.[7–11]

Spin–orbit interaction is a relativistic effect that occurs when a quantum mechanical particle with a non-zero spin moves in a region with a non-zero electric field originating a magnetic component in the rest frame of the electron. The presence of this effective magnetic field affects both the dynamics of the spin and the total energy of the electron and such interaction is called SO coupling that leads to the relaxation of the electron spin. The static electric field that causes the SO interaction can have different physical origins, for example being the electric field of the atomic nucleus, or related to the crystal or the band structure of the solid.

Two main spin relaxation mechanisms were found to be the most relevant for conduction electrons in metals and semiconductors: Elliot–Yafet (EY) and D'yakonov–Perel (DP).[12] The EY process leads to spin-relaxation due to electron scattering on impurities in the presence of SO coupling while the DP mechanism arises from the spin-splitting of carrier spectra in noncentrosymmetric media.[13] The SO can also be separated into two terms named Rashba (caused by the asymmetry of the quantum well or heterojunction) and Dresselhaus (arises from the lack of inversion in the original crystal).

There are many evidences that Rashba term gives a bigger contribution to the splitting in the case of narrow-gap heterostructures due to the strong SO interaction.[14–17] In the particular case of the IV–VI lead-salt semiconductors, just a few studies had been carried out.[18,19] From the basic physics research point of view, PbTe quantum wells (QWs) present an advantage as compared to the other III–V based structures since its lead-salt crystalline structure presents bulk inversion symmetry. Hence, the SO splitting in such structures is purely Rashba instead of a mixture of Rashba and Dresselhaus, commonly observed in III–V compounds. In addition, the multiple applications of PbTe and its unique physical properties make it an attractive research subject. Its applications include infrared sensors[20] and thermoelectric devices.[21,22] Recently, spin Hall effect (SHE) has being theoretically predict to manifest in IV–VI structures,[23,24] but so far, experiments did not succeed to confirm such prediction.[25] In addition, $Pb_{1−x}Sn_xTe$ films have being identified as topological crystalline insulators, i.e., specific crystalline symmetries warrant the topological protection of metallic surface states. In general, in these new quantum materials, time-reversal symmetry and strong spin–orbit effects require that the bulk insulating states are accompanied by metallic helical Dirac-like electronic states on the surface of the crystal.[26] For the case of $Pb_{1−x}Sn_xTe$, the topological phase is possible due to the strong spin-orbit coupling present in PbTe associated to the decrease of the energy gap as the Sn content increases leading to a band inversion.[27] These new results demand a deeper investigation in SO coupling effect on IV–VI compounds.

To probe the SO coupling effect, weak antilocalization (WAL) phenomenon has been considered as one powerful tool and is commonly used to obtain the SO and inelastic scattering times in films and QWs.[28] Weak localization is a quantum effect that arises from the quantum interference between the electronic wave functions moving in the same path but in opposite directions. Its suppression by SO coupling gives rise to the phenomenon known as weak antilocalization which manifests itself as a negative magnetoconductance at low fields.

In this work, we report an experimental investigation performed on two *n*-type PbTe/PbEuTe QWs where the SO coupling effect was probed through weak antilocalization effect. For the analysis, the multivalley and anisotropic

TABLE I. Data of the PbTe/Pb$_{1-x}$Eu$_x$Te quantum well samples: Eu content x, thickness of the buffer layer (t^{buffer}), thickness of the n-type Pb$_{1-x}$Eu$_x$Te barrier layer doped with bismuth ($t^{barrier}$), thickness of the PbTe well (t^{well}), sheet electron concentration n and Hall mobility μ measured in the temperature T range.

Sample	x	t^{buffer} (μm)	$t^{barrier}$ (nm)	t^{well} (nm)	T range (K)	n (10^{15} m^{-2})	μ (m^2/Vs)
ID7111	0.10	2.7	30.8	14.5	1.2–10.0	5.0–4.3	1.65–1.47
ID6072	0.12	2.4	30.0	10.0	1.2–10.0	1.3–0.8	0.80–0.60

character of PbTe was also taken into account in order to calculate the Fermi energy and energy subbands and we found that only the first subband of the 1st longitudinal valley is occupied. Using the model developed by Hikami, Larkin, and Nagaoka (HLN),[29,30] it was possible to extract the inelastic and SO scattering times and calculate the strength of the zero field spin-splitting energy (Δ_{so}), which depends linearly on the Fermi wave vector k_F. The results confirm theoretical predictions of large Rashba SO effect on PbTe/PbEuTe QWs and enhance the possibility of application of these structures on the development of spintronic devices.

II. SAMPLE STRUCTURE AND EXPERIMENTAL SETUP

The PbTe/Pb$_{1-x}$Eu$_x$Te quantum well samples were grown by molecular beam epitaxy on (111) cleaved BaF$_2$ substrates. The sample structure consisted of a 2 to 3 μm thick Pb$_{1-x}$Eu$_x$Te buffer layer grown on top of the (111) BaF$_2$ substrate followed by a PbTe well embedded between two Pb$_{1-x}$Eu$_x$Te barriers doped with bismuth, which guarantee an n-type character for these samples.

For these experiments, two PbTe/Pb$_{1-x}$Eu$_x$Te QW samples with In contacts in the Van der Pauw geometry were electrically characterized. The structural and electrical data of the samples ID7111 and ID7062, used in this work, are displayed in Table I.

The experiments were carried out at low temperatures (1.2–8.0 K) using a liquid ^{4}He cryostat with a superconducting magnet. The magnetoresistance was measured using phase-sensitive detection with 1 μA quasi-dc currents at 10.6 Hz.

III. RESULTS AND DISCUSSION

For magnetoresistance measurements we have averaged over the magnetic field directions using $R_{xx} = [R(B) + R(-B)]/2$ to eliminate any Hall component. Figures 1(a) and 1(b) present the magnetoconductivity (MC) curves (open points) obtained for samples ID7111 and ID6072 for temperatures between 1.2 K and 10.0 K and for magnetic fields in the range of -100 mT to $+100$ mT. Not all the measured curves are present in this figure in order to obtain a better visualization. The negative MC amplitudes are a clear signature of the weak antilocalization effect and show the presence of SO coupling in both samples. It is also possible to observe that the MC amplitudes scale with temperature.

In order to investigate the origin of the SO coupling effect observed in these PbTe QWs, we use the HLN model to extract the SO and inelastic scattering times by fitting the HLN function to the measured data using a global optimization procedure. The HLN model can be written as follows:[29,30]

$$
\Delta\sigma = -\frac{e^2}{2\pi h}\left[\psi\left(\frac{B_i}{B}+\frac{1}{2}\right) - \ln\left(\frac{B_i}{B}\right)\right]
$$
$$
-\frac{e^2}{\pi h}\left[\psi\left(\frac{B_{SO}+B_e}{B}+\frac{1}{2}\right) - \ln\left(\frac{B_{SO}+B_e}{B}\right)\right]
$$
$$
+\frac{3e^2}{2\pi h}\left[\psi\left(\frac{(4/3)B_{SO}+B_i}{B}+\frac{1}{2}\right) - \ln\left(\frac{(4/3)B_{SO}+B_i}{B}\right)\right],
$$
(1)

where B_{SO} is the SO field, B_i is the dephasing field, and B_e is the elastic field. We also derived the mean free path l ($\sim$170.0 nm and 40.0 nm for samples ID7111 and ID6072,
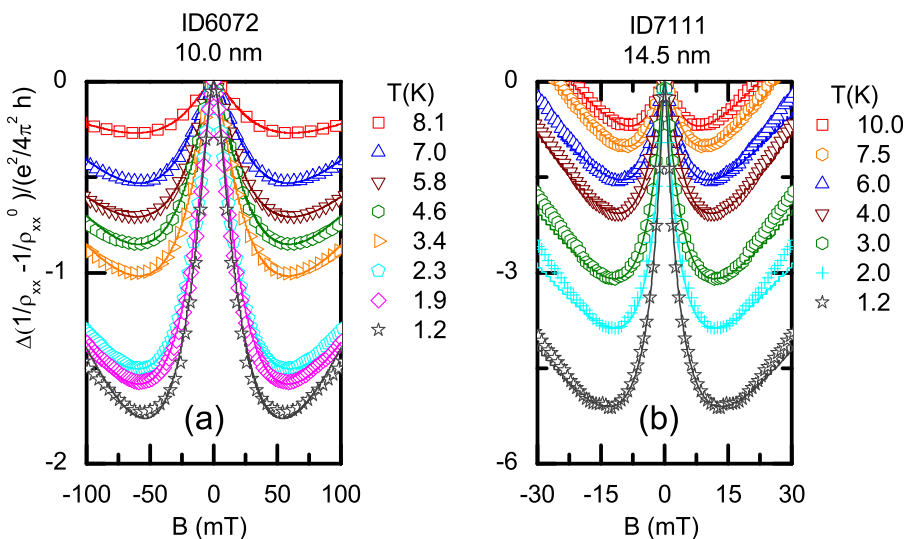

FIG. 1. Magnetoconductivity measured data (open points) and best fitted curves (solid lines), obtained for the PbTe/Pb$_{1-x}$Eu$_x$Te quantum well samples (a) ID6072 and (b) ID7111, as a function of magnetic fields from -100 mT to $+100$ mT at different temperatures from 1.2 K to 10.0 K. The wider minima separation in magnetoconductance for sample ID6072 indicates stronger SO coupling.

respectively) and found it is smaller than the magnetic length $l_B = \sqrt{\hbar/eB}$ ($\sim$200 nm for $B \sim 100$ mT) indicating that the HLN model is applicable in the magnetic field range where the analysis was performed as will be seen next.

The complex nature of the HLN model, due to its non-linear relation between the four independent parameters, usually leads to complicated parameter space. Fitting procedures, based on the Levenberg-Marquardt techniques, typically result in sub-optimal parameters, which are mostly dependent on initial guesses. To circumvent this situation, we have applied a powerful statistical technique recently developed to deal with multi-extremal problems involving optimization: the cross-entropy (CE) method.

The CE analysis was originally used in the optimization of complex computer simulation models involving rare event simulations,[31] having been modified by Rubinstein[32] to deal with continuous multi-extremal and discrete combinatorial optimization problems. Its theoretical asymptotic convergence has been demonstrated by Margolin,[33] while Kroese et al.[34] studied the efficiency of the CE method in solving continuous multi-extremal optimization problems. Some examples of robustness of the CE method in several situations are listed in Ref. 35. The CE method has been also applied to many complex astrophysical problems as discussed in Refs. 36 and 37.

The basic procedures involved in the CE optimization can be summarized as follows:[34] (i) random generation of the initial parameter sample, obeying pre-defined criteria; (ii) selection of the best samples based on some mathematical criterion; (iii) random generation of updated parameter samples from the previous best candidates to be evaluated in the next iteration and, (iv) optimization process repeats steps (ii) and (iii) until a pre-specified stopping criterion is fulfilled.

We have applied this procedure to fit the HLN function to our experimental data. To quantify the goodness of fit, we adopt a simple Gaussian likelihood function such that

$$L(B_{so}, B_i, B_e, C \vee \Delta R_i) \propto \prod e^{\left[\frac{(M_i(B_{so}, B_i, B_e, f) - \mu_i)^2}{\sigma_i^2}\right]},$$

where L is the likelihood written as usual for the Maximum likelihood problem, M_i is the HLN model to be fit to the magnetoresistance data ΔR_i for the ith B field strength observed. The observed uncertainty of the data is given by σ_i. In our case, we have assumed that all measurements have equal uncertainty which we set to one. The free parameters are the SO field (B_{so}), the dephasing time field (B_i) and a multiplicative constant f introduced in the model to account for possible multichannel conduction. The parameter space defined for each fit varied slightly but in general was within the following range: B_{so} from 1.0×10^{-6} T to 50×10^{-3} T for sample ID6072 and from 1.0×10^{-6} T to 10.0×10^{-3} T for sample ID7111, B_i from 1.0×10^{-6} T to 1.0×10^{-3} T for samples ID7111 and from 1.0×10^{-6} T to 10.0×10^{-3} T for sample ID6072 and f from 0.1 to 5. B_e was not considered as a fitting parameter and its values were calculated from the transport measurements (see Table I) and are presented in Table II.

TABLE II. Spin-orbit field (B_{so}), dephasing time field (B_i), elastic field (B_e), and multiplicative constant f obtained form a best-fit procedure at different temperatures from 1.2 K to 7.5 K for the PbTe/Pb$_{1-x}$Eu$_x$Te quantum well samples ID6072 and ID7111.

	ID6072				ID7111			
T (K)	B_i (mT)	B_{so} (mT)	B_e (mT)	f	T (K)	B_i (mT)	B_{so} (mT)	B_e (mT)	f
1.2	2.92	12.4	127	2.7	1.2	0.20	2.8	8.6	3.2
1.4	2.68	12.5	129	2.4	1.5	0.21	2.6	8.8	3.2
1.6	2.62	12.9	131	2.2	1.6	0.20	2.5	9.1	3.0
1.9	2.66	13.3	131	2.1	2.0	0.21	2.5	10.1	2.6
2.3	2.05	12.7	132	1.6	2.5	0.22	2.6	10.7	3.2
2.7	2.70	13.2	131	2.2	3.0	0.34	2.5	11.1	2.9
3.4	3.32	13.5	198	1.6	3.5	0.39	2.4	11.5	2.9
4.6	4.10	14.0	204	1.7	4.0	0.61	2.5	12.7	3.3
5.1	4.18	14.3	211	1.6	6.0	0.46	2.3	12.9	2.3
7.0	4.92	14.1	233	1.1	7.5	0.81	2.2	12.8	2.7
8.1	5.00	14.8	313	0.64	10.0	0.86	2.05	12.8	2.2

The best fit parameters obtained for the two PbTe/Pb$_{1-x}$Eu$_x$Te QW samples as a function of temperature are shown in Table II.

We have also explored the confidence intervals of the fits obtained. To accomplish this we have performed a Monte-Carlo procedure to probe the parameter space based on a uniform distribution and calculate the likelihood function. The sample points were then used to estimate 1σ, 2σ, and 3σ confidence intervals. The final contour plots with the confidence intervals obtained for the parameter pair (B_{so}, B_i), setting the remaining parameters to their best fit values, are shown in Figure 2. We have not plotted the other pair combinations since (B_{so}, B_i) are the main ones.

We point out that initially the fits were performed without the multiplicative constant f. However, in all temperatures for all samples studied, the fits obtained without the constant were considerably worse than the fits with the added free parameter.

The solid lines in Figures 1(a) and 1(b) correspond to best fitted curves to the experimental data, when applying the fitting procedure describe above. The scattering times can be derived from the fitting parameters presented in Table II according to the relation $\tau_j = \hbar/4eDB_j$, where $j = so, e, i$, and D is the diffusion constant. Figure 3(a) presents the log plot of the inelastic scattering time τ_i, obtained from the best fitted curves of Figure 1, as a function of temperature. For temperatures higher than $\sim$2 K, the temperature dependence of inelastic scattering time behaves like $\tau_i \propto T^{-0.75}$ and $\tau_i \propto T^{-0.72}$ for samples ID7111 and ID6072, respectively. It is known that electron–electron interaction, involving small energy transfer at each scattering event, has a temperature dependence such that $\tau_i \propto T^{-1.0}$,[38] suggesting that this can be the main inelastic scattering mechanism in these PbTe QWs. In fact, measurements performed in PbTe quantum point contacts suggest that electron-electron interaction may play an important role despite the large dielectric constant ($\varepsilon_0 \sim 1400$ at $T = 4.2$ K).[39] Figure 3(b) shows the SO scattering time (τ_{so}) as a function of temperature. The τ_{so} values for sample ID6072 are nearly constant if one does not consider
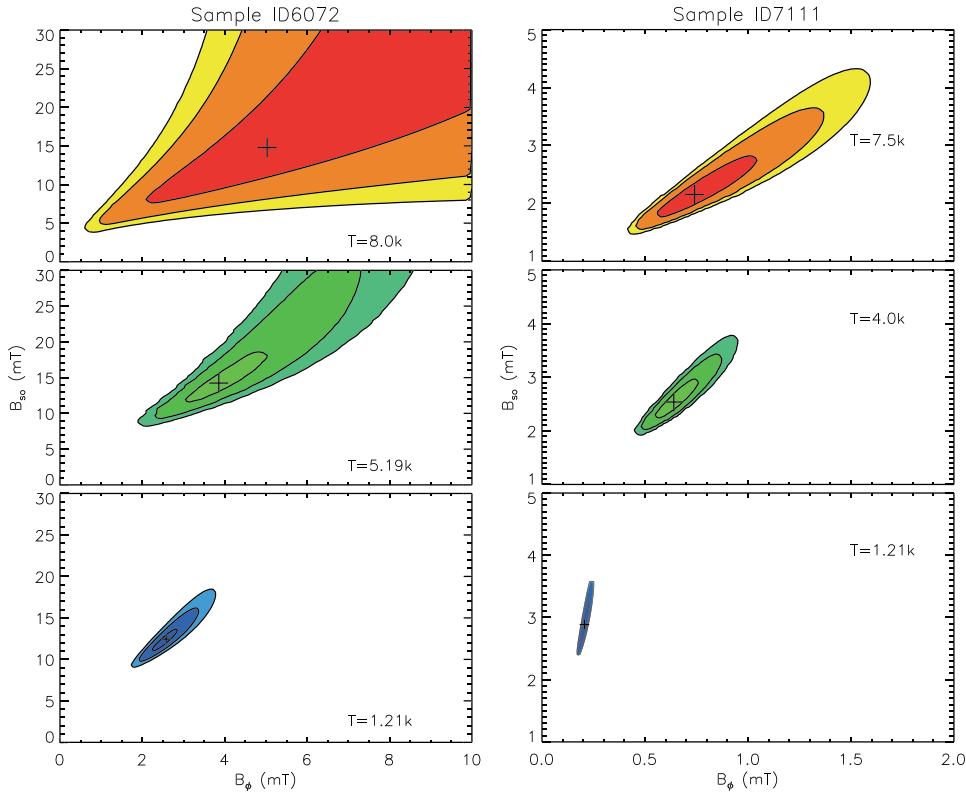
FIG. 2. Contour plots with 1σ, 2σ, and 3σ confidence intervals obtained for the parameter pair (B_{so}, B_i). Crosses mark the best parameters fit values for sample ID6072 in the left column and for sample ID7111 in the right column.

the two points out of the curve, while for sample ID7111 values slightly decrease as temperature decreases. For the DP mechanism the dependence $\tau_{so} \propto \tau_e^{-1.0}$ is expected.[40] The inset in Figure 3(b) presents the log plot of τ_{so} as a function of τ_e and shows $\tau_{so} \propto \tau_e^{-1.7}$ for samples ID7111 and $\tau_{so} \propto \tau_e^{-2.2}$ for samples ID6072. This deviation from DP model can indicate that an additional contribution to SO is present or that the model cannot properly describe the effects in these samples. From Figure 3(b) we also found that the values of τ_{so} are smaller for sample ID6072 as compared to
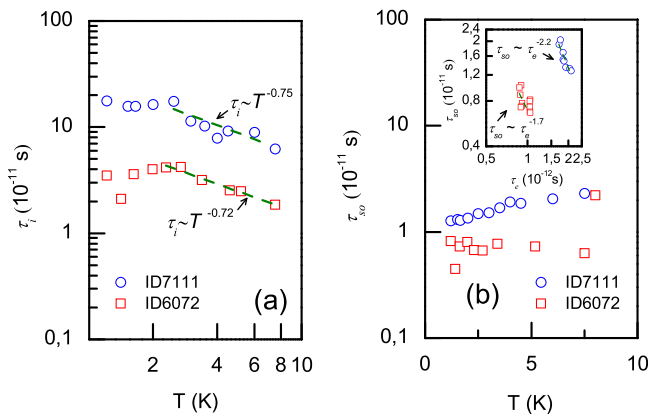
those found to sample ID7111, indicating that the SO coupling is stronger for sample ID6072. This verification also agrees with the wider minima separation in magnetoconductance found for this sample (see Figure 1).

In addition, from elastic and inelastic scattering times it is possible to estimate the intensity of the zero field spin-splitting energy due to SO interaction according to the relation[41] $\Delta_{so} = \sqrt{2}\hbar(\tau_e\tau_{so})^{-\frac{1}{2}}$, where τ_e is the elastic scattering time, which was obtained from the mobility values presented in Table I. The values of Δ_{so} are presented in Figure 4(a) as a function of the Fermi wave vector ($k_F = \sqrt{2\pi n}$) that varies with temperature according to n as shown in Table I.
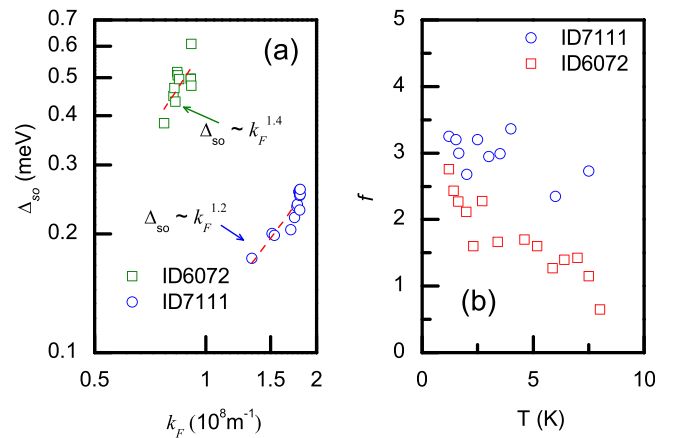

FIG. 3. Temperature dependence of (a) inelastic τ_i and (b) spin-orbit τ_{so} scattering times, as obtained from the best fitted curves of Figure 1. For temperatures higher than ~2K, the inelastic scattering time for samples ID7111 and ID6072 behaves like $\tau_i \propto T^{-0.75}$ and $\tau_i \propto T^{-0.72}$, respectively. These dependencies suggest that electron-electron interaction is the main inelastic scattering mechanism in these PbTe QWs. The values of τ_{so} are smaller for sample ID6072 as compared to those found to sample ID7111, indicating that the SO coupling is stronger for sample ID6072. The inset presents the log plot of τ_{so} as a function of τ_e and shows $\tau_{so} \propto \tau_e^{-1.7}$ for samples ID7111 and $\tau_{so} \propto \tau_e^{-2.2}$ for samples ID6072 (see text for further explanation).

FIG. 4. (a) Zero field spin-splitting energy Δ_{so} as a function of the Fermi wave vector k_F for the PbTe/Pb$_{1-x}$Eu$_x$Te QW samples. The log plot shows $\Delta_{so} \sim k_F^{1.2}$ and $\Delta_{so} \sim k_F^{1.4}$ dependencies for samples ID7111 and ID6072, respectively, indicating that the Rashba effect should be the main mechanism responsible for the spin-orbit interaction. (b) The values of the fitting parameter f as a function of temperature for both samples.

According to the Rashba spin splitting theory, the energy splitting has a linear dependency on k_F and is given by $\Delta_R = \alpha k_F$, where α is the coupling parameter. The log plot in Figure 4(a) shows $\Delta_{so} \sim k_F^{1.2}$ and $\Delta_{so} \sim k_F^{1.4}$ for samples ID7111 and ID6072, respectively. This result indicates that the Rashba effect should be the main mechanism responsible for the SO interaction observed in these samples, in agreement with the theoretical predictions for zero field energy splitting in IV–VI QWs.[18,19] The values of Δ_{so} varied from 0.38 meV to 0.60 meV for sample ID6072 and from 0.17 meV to 0.26 meV for sample ID7111. These values are of the same order of magnitude found for GaAs/Al$_x$Ga$_{1-x}$As (0.17–0.26 meV) and In$_x$Ga$_{1-x}$As/InP (0.5–0.8 meV) QWs.[2,7] The values found in the QWs investigated in this work are also close to values theoretically predicted for asymmetric CdTe/PbTe/PbSrTe QWs if only the first subband for the longitudinal valley is occupied.[42] We show next that this is the case of the QWs investigated here.

It is still necessary to discuss why good fits using the HLN model are possible only if f parameter is introduced. Figure 4(b) exhibits the values of f for the samples investigated as a function of temperature. For sample ID7111, the f values oscillate between 2.5 and 3.0, approximately. For sample ID6072, one can observe a plateau around 1.5 between 2.0 K and 7.0 K, and an increasing of the f factor that reaches 2.7 as temperatures decreases below 2.0 K. The reduced form of HLN model also contains a prefactor $\alpha = -1/2$ for each subband that carries a π Berry phase.[43] In the weak interband coupling limit, multiple independent bands should add up to give a bigger value of α, i.e., $\alpha = -1.0$ indicates two carrier channels. For PbTe/PbEuTe QWs, multivalley transport is possible if the oblique and longitudinal valleys participate of the electrical transport depending on the position of the Fermi level (ε_F). Following the procedure described in Ref. 39, we were able to calculate the confinement energies of the longitudinal and oblique valleys in the 10.0 nm and 14.5 nm QWs. For the 10.0 nm QW, the energies are 11, 38, 78, 123, 170, and 219 meV for the longitudinal valley and 45 and 154 meV for the oblique valley. The energies calculated for the 14.5 nm QW are 5, 22, 45, 73, 105, 139, 173, and 207 meV for the longitudinal valley and 28, 102, and 192 meV for the oblique valley.

Using the two-dimensional density of states, one can derive the approximate ε_F integrating over all possible subbands to obtain the carrier density, i.e., $n = \sum_{i,l,\sigma} \int_0^{\varepsilon_F} D(E)dE$, where i is the number of confinement energies already computed, l is the subband degeneracy, and σ is the spin degeneracy. For this calculation, we considered the average carrier concentration for both samples and obtained $\varepsilon_F = 14$ meV and $\varepsilon_F = 12$ meV for samples ID6072 and ID7111, respectively. These Fermi energies demonstrate that only the first longitudinal valley is occupied in both quantum wells and, therefore, the values higher than unity for the f factor obtained here are not originated from contribution from additional subbands.

On the other hand, it is possible that contributions for SO coupling come from the QWs barriers, leading to f values higher than unity. For n-type Pb$_{1-x}$Eu$_x$Te:Bi films, a metal insulator transition occurs for $x \sim 0.1$.[44] This indicates that the QW barriers in sample ID7111 are not completely insulators, but probably have a metallic phase that co-exists next to the insulator region. This explains the higher values of f in this sample and values closer to unity for sample ID6072, where the barriers are farther from the insulator region.

IV. CONCLUSIONS

In this work, we presented the experimental investigation of SO coupling effect in n-type PbTe QWs by means of weak antilocalization phenomena and confirmed the theoretical predictions of the existence of large Rashba effect in these systems. For the analysis of the experimental data, we made use of a global optimization computational method to perform the fit of the complex HLN function to the experimental data. We also verified that possible contributions from the barriers can occur and that the HLN model can take into account these contributions by introducing a multiplying factor f as an additional free parameter. The electron-electron interaction seems to be the dominating scattering mechanism in these QWs. The zero field spin-splitting energy Δ_{so} observed in this work is of the same order as compared to the values found to other semiconductor compounds, also in agreement with predicted values for PbTe QWs. These results obtained from the detailed analysis presented in this work enhance the possibility of application of IV–VI compounds on the development of spintronic devices.

[1]B. Grbic, R. Leturcq, T. Ihn, K. Ensslin, D. Reuter, and A. D. Wieck, Phys. Rev. B **77**, 125312 (2008).
[2]S. A. Studenikin, P. T. Coleridge, G. Yu, and P. J. Poole, Semicond. Sci. Technol. **20**, 1103 (2005).
[3]J. B. Miller, D. M. Zumbuhl, C. M. Marcus, Y. B. Lyanda-Geller, D. Goldhaber-Gordon, K. Campman, and A. C. Gossard, Phys. Rev. Lett. **90**, 076807 (2003).
[4]I. Zutic, J. Fabian, and S. Das Sarma, Rev. Mod. Phys. **76**, 323 (2004).
[5]G. A. Prinz, Science **282**, 1660 (1998).
[6]B. Datta and S. Das, Appl. Phys. Lett. **56**, 665 (1990).
[7]W. Desrat, D. K. Maude, Z. R. Wasilewski, R. Airey, and G. Hill, Phys. Rev. B **74**, 193317 (2006).
[8]X. Z. Liu, G. Yu, L. M. Wei, T. Lin, Y. G. Xu, J. R. Yang, Y. F. Wei, S. L. Guo, J. H. Chu, N. L. Rowell, and D. J. Lockwood, J. Appl. Phys. **113**, 013704 (2013).
[9]J. Balakrishnan, G. K. W. Koon, M. Jaiswal, A. H. C. Neto, and B. Özyilmaz, Nat. Phys. **9**, 284 (2013).
[10]A. M. Gilbertson, M. Fearn, J. H. Jefferson, B. N. Murdin, P. D. Buckle, and L. F. Cohen, Phys. Rev. B **77**, 165335 (2008).
[11]G. Yu, N. Dai, J. H. Chu, P. J. Poole, and S. A. Studenikin, Phys. Rev. B **78**, 035304 (2008).
[12]A. Tackeuchi, T. Kuroda, S. Muto, Y. Nishkawa, and O. Wada, Jpn. J. Appl. Phys. **38**, 4680 (1999).
[13]W. Knap, C. Skierbiszewski, A. Zduniak, E. Litwin-Staszewska, D. Bertho, F. Kobbi, and J. L. Robert, Phys. Rev. B **53**, 3912 (1996).
[14]S. D. Ganichev, V. V. Belkov, L. E. Golub, E. L. Ivchenko, P. Schneider, S. Giglberger, J. Eroms, J. DeBoeck, G. Borghs, W. Wegscheider, D. Weiss, and W. Prettl, Phys. Rev. Lett. **92**, 256601 (2004).
[15]E. A. de Andrada e Silva, Brazilian Journal of Physics **26**, 1 (1996).
[16]G. Lommer, F. Malcher, and U. Rossler, Phys. Rev. Lett. **60**, 728 (1988).

[17]J. Luo, H. Munekata, F. F. Fang, and P. J. Stiles, Phys. Rev. B **41**, 7685 (1990).

[18]M. M. Hasegawa and E. A. de Andrada e Silva, Phys. Rev. B **68**, 205309 (2003).

[19]M. M. Hasegawaa, E. A. de Andrada e Silva, and G. C. La Rocca, Physica E **20**, 400 (2004).

[20]A. S. Barros, E. Abramof, and P. H. O. Rappl, J. Appl. Phys. **99**, 024904 (2006).

[21]Y. Pei, A. LaLonde, S. Iwanaga, and G. J. Snyder, Energy Environ. Sci. **4**, 2085 (2011).

[22]V. A. da Costa and E. A. de Andrada e Silva, Phys. Rev. B **82**, 153302 (2010).

[23]A. Dyrdal, V. K. Dugaev, and J. Barnas, EPL **85**, 67004 (2009).

[24]S. Murakami, N. Nagaosa, and S.-C. Zhang, Phys. Rev. Lett. **93**, 156804 (2004).

[25]K. A. Kolwas, G. Grabecki, S. Trushkin, J. Wróbel, M. Aleszkiewicz, Ł. Cywiński, T. Dietl, G. Springholz, and G. Bauer, Phys. Status Solidi B **250**, 37 (2013).

[26]P. Dziawa, B. J. Kowalski, K. Dybko, R. Buczko, A. Szczerbakow, M. Szot, E. Łusakowska, T. Balasubramanian, B. M. Wojek, M. H. Berntsen, O. Tjernberg, and T. Story, Nat. Mater. **11**, 1023 (2012).

[27]E. Abramof, S. O. Ferreira, P. H. O. Rappl, H. Closs, and I. N. Bandeira, J. Appl. Phys. **82**(5), 2405 (1997).

[28]G. Bergmann, Phys. Rep. **107**, 1 (1984).

[29]S. Hikami, A. I. Larkin, and Y. Nagaoka, Prog. Theor. Phys. **63**, 707 (1980).

[30]B. A. Assaf, T. Cardinal, P. Wei, F. Katmis, J. S. Moodera, and D. Heiman, Appl. Phys. Lett. **102**, 012102 (2013).

[31]R. Y. Rubinstein, Eur. J. Oper. Res. **99**, 89 (1997).

[32]R. Rubinstein, Methodology and Computing in Applied Probability **1**, 127 (1999).

[33]L. A. Margolin, Ann. Operations Res. **134**, 201 (2005).

[34]D. P. Kroese, S. Porotsky, and R. Y. Rubinstein, Methodol. Comput. Appl. Probab. **8**, 383 (2006).

[35]P. T. de Boer, D. P. Kroese, S. Mannor, and R. Y. Rubinstein, Ann. Oper. Res. **134**, 19 (2005).

[36]A. F. Oliveira, H. Monteiro, W. S. Dias, and T. C. Caetano, Astron. Astrophys. **557**, A14 (2013).

[37]A. Caproni, Z. Abraham, and H. Monteiro, Mon. Not. R. Astron. Soc. **428**, 280 (2013).

[38]B. L. Altshuler, A. G. Aronov, and D. E. Khmelnitzkii, J. Phys. C **15**, 7367 (1982).

[39]V. A. Chitta, W. Desrat, D. K. Maude, B. A. Piot, N. F. Oliveira, Jr., P. H. O. Rappl, A. Y. Ueta, and E. Abramof, Phys. Rev B **72**, 195326 (2005).

[40]P. D. Dresselhaus, C. M. A. Papavassiliou, R. G. Wheeler, and R. N. Sacks, Phys. Rev. Lett. **68**, 106 (1992).

[41]S. Kettemann, Phys. Rev. Lett. **98**, 176808 (2007).

[42]S. Jin, H. Wu, and T. Xu, Appl. Phys. Lett. **95**, 132105 (2009).

[43]H.-Z. Lu and S.-Q. Shen, Phys. Rev. B **84**, 125138 (2011).

[44]A. Prinz, G. Brunthaler, Y. Ueta, G. Springholz, G. Bauer, G. Grabecki, and T. Dietl, Phys. Rev. B **59**, 12983 (1999).